Electronic Supplemental Material for

Thermoplastic Building Blocks for the Fabrication of Microfluidic Masters

Michael A. Stoller,[a] Abhiteja Konda,[a] Matthew A. Kottwitz,[a] and Stephen A. Morin*[ab]

[a] Department of Chemistry, University of Nebraska-Lincoln, Lincoln, NE 68588.
[b] Nebraska Center for Materials and Nanoscience, University of Nebraska-Lincoln, Lincoln, NE 68588.

* To whom correspondence should be addressed. E-mail: smorin2@unl.edu.

Materials and Methods

A. Materials

The microfluidic stamps were fabricated in polydimethylsiloxane (PDMS, Sylgard® 184) purchased from Dow Corning Co. Water-soluble dyes (in various concentrations) were prepared using Tartrazine-FD&C Yellow #5 (CAS 1934-21-0), Allura Red AC-FD&C Red #40 (CAS 25956-17-6), Fast Green FCF-FD&C Green #3 (CAS 2353-45-9), and Indigo Carmine-FD&C Blue #2 (CAS 860-22-0) purchased from VWR®. Mineral oil (CAS 8042-47-5), Tween 20® (CAS 9005-64-5), ammonium iron(II) sulfate hexahydrate 99% (CAS 7783-85-9), 1,10-phenanthroline monohydrate 99+% (CAS 5144-89-8), hydroxylamine hydrochloride (CAS 5470-11-1), sodium acetate anhydrous, 99% (CAS 127-09-3), and 1H,1H,2H,2H-perfluorooctyltrichlorosilane (CAS 78560-45-9) were purchased from Fisher Scientific®. Aquapel (CAS 64742-47-8) was purchased from Amazon®. Iron unknowns (CAS 1309-37-1) were purchased from Thorn Smith Laboratories. LabSilicone/polyethylene (PE) tubing (Masterflex Tygon® Lab E-3603 tubing, and PE tubing, Intramedic™ PE60 and PE160 by BD & Co.) were purchased from Fisher Scientific®. Heat-resistant borosilicate glass substrates of varied thickness and dimensions (l×b×h, 8×8×0.25 in. P/N 8476K185, 5×3×0.25 inch P/N 8476K43, and 3×3×0.188 inch P/N B84815430), and Teflon film (0.003" thick, P/N 8569K14) were purchased from McMaster-Carr®. Original, clear, Krazy® glue was purchased from Office Depot®.

Methods

B. Fabrication of masters and microfluidic devices

B1. Design and printing of building blocks: We fabricated the building blocks using solid object printing.[1] The straight and circular components were designed in a CAD program and printed in ABS using a 3D-printer (Dimension Elite, Stratasys Ltd.). The technical drawings of the components are shown in Fig. 2A of the maintext.

B2. Device fabrication:

B.2.1. Masters

Permanent assembly of masters via thermal pressing and welding: ABS building blocks were heated between two glass plates using a convection oven at 190° C for 12 minutes to smooth and remove imperfections on the surfaces of the ABS blocks that result from the extrusion based 3D printing process. After the initial press, the ABS building blocks were cooled for at least 10 minutes at -20° C and then arranged on a glass substrate in the desired geometry at room temperature. The arranged set of blocks were covered with a second glass plate and then heated at 190° C for 13 minutes "welding" the individual blocks into a single structure—the ABS blocks were slightly compressed in the z direction and therefore expand in the x and y directions (Fig. S1) causing the interface between touching blocks to fuse together when they were heated.

We also produced masters to fabricate microfluidic devices with variable height channels by stacking and welding the individual blocks after the initial press of 12 minutes at 190° C, we placed one block on top of the other and heated them for 6 minutes at 190° C (without applying compression) to weld the blocks into a master (Fig. 4B of the maintext).

Building block placement: Grid paper with 5 mm by 5 mm squares was used to aid the process of assembling thermoplastic building blocks into desired geometries precisely on glass. Grid paper was placed under the glass substrate and was used as a visual guide. Grid paper is sufficient for most demonstrations of simple geometries; when added precision and reproducibility were desired, a stencil was used as a template during assembly. We used a laser cutter (Epilog Fusion 32) to fabricate stencils from thin sheets of heat-resistant Teflon®. To demonstrate stencil-based fabrication, we produced seven replicate masters with T-shaped and 45° angled junctions using a stencil and compared them to masters generated using a grid pattern (Fig. S2). We then analyzed the angle between the welded blocks (using ImageJ). The average angle for masters with 45° junctions was 46.0 ± 2° (Fig. S2A-B, E) using a template and 49.3 ± 4° (Fig. S2E) using only a grid; the average angle for masters with 90° junctions was

90.1 ± 0.6° (Fig. S2C-D, E) and 90.3 ± 0.7° (Fig. S2E) using only a grid. We note that while there was only a marginal improvement in accuracy for right angle junctions when stencils were used versus grid-guided placement (because this geometry was "natural" for rectilinear blocks) we could more rapidly assemble such junctions using stencils. Stencils of more complex geometries useful for the fabrication of devices with various angles between channels could be fabricated following this approach (or others, e.g., blade-equipped plotters or craft cutters).

Reversible assembly of masters from building blocks: We also fabricated microfluidic devices using combinations of standard building blocks (or thermally welded combinations of blocks) without permanently fusing them together. We used a silanized (with a perfluorinated trichlorosilane) PDMS substrate as a base layer on which the building blocks were arranged, cast in PDMS, and demolded. Silanized PDMS substrates were prepared by oxidizing native PDMS in oxygen plasma for 30 seconds at % RF power 60, followed by exposing the oxidized PDMS to 1H,1H,2H,2H-perfluorooctyltrichlorosilane for 1 hour under vacuum. As the blocks were not permanently fused they could be separated, and then rearranged in a different layout to fabricate a new device. This method allows the same building blocks to be used several times resulting in a range of micro-channel geometries.

B.2.2. Casting in PDMS and curing: The masters, either directly printed, thermally welded, or reversibly assembled were placed on a glass substrate (or left on the silanized PDMS support in the case of reversible assembly) and covered with PDMS liquid pre-polymer with a 10:1 base:catalyst ratio and cured at 60° C for 60 minutes. After curing, the PDMS was carefully peeled off the glass substrate (or PDMS support) and the ABS masters removed.

B.2.3. Sealing via O_2 plasma-activated bonding: The PDMS stamps were sealed to glass by plasma-activated bonding. A clean glass substrate and the PDMS stamp (open channels facing up) were exposed to oxygen plasma for 30 seconds at 60 % power in a plasma etcher (Plasma Etch Inc., Carson City, NV, Model# PE-25 Series). The plasma exposed surfaces of the device and the substrate were brought into conformal contact for bonding.[2] The device was then baked in an oven at 80° C for at least 15 minutes to ensure the PDMS was fully bonded to the glass and the channels were sealed completely.

B.2.4. Inlets/Outlets: Inlets/outlets were created using a 1 mm biopsy punch. PE-60 tubing was used to connect the inlets/outlets to pumps (either peristaltic pump, MasterFlex L/S Cole-palmer, or syringe pumps, KD Scientific Legato Series 210 and New Era NE-4000) to flow solutions through the devices.

B3. Geometric changes associated with thermal pressing/welding

We determined the change in the cross-sectional dimensions of the building blocks associated with thermal pressing/welding using optical profilometry (Scantron, Proscan 1000). The thermal pressing was carried out by placing the ABS building blocks between glass plates (3 in. × 3 in.) and heating at 190° C for different times that mimic the experimental procedure used to fabricate masters by welding building blocks: (i) 12 minutes (to smooth and remove imperfections from the surface), (ii) 25 minutes (a smoothing step followed by an additional 13 minutes to weld), (iii) 30 minutes (a smoothing step and welding step with an additional 5 minutes of pressing), and (iv) 35 minutes (a smoothing step and welding step with an additional 10 minutes of pressing). We fabricated seven replicates for each of the conditions described above and characterized them along with seven replicates of the as-printed blocks. A step size resolution of 0.01 mm (x and y axis), and an average of four scans was used to profile these blocks. We then used MATLAB to analyze the data and determine the height and width of the channels (Fig. S1).

B4. Stability of thermally welded building blocks

The set of building blocks used in this paper was fabricated by heating the as-printed blocks for 12 minutes at 190° C between two glass plates (“pressing”) to smooth and remove imperfections from the surface. The smooth blocks were then aligned in the desired geometry and thermally welded through a secondary step for 13 minutes at 190° C to produce a master. We determined the stability (load at breakage) of the welded blocks using a materials testing system (Instron® 5944, 2kN capacity). We compared the load required to break masters of 3 cm in length that were obtained by welding two straight blocks that were 1.5 cm long in a head to head fashion, with as-printed blocks that were 3 cm long and thermally pressed for 25 minutes (to mimic the welding procedure used in master fabrication). We found that the head to head welds fractured at 0.1 ± 0.01 N of tensile force while the solid blocks required 4.6 ± 0.2 N of tensile force (Fig. S2).

The thermal welds were analyzed to determine the dimensions at the weld using confocal microscopy (Keyence VK-X200 series). Seven replicates of three different types of welds (head-to-head and "T" configurations involving straight-curved or straight-straight junctions) were analyzed using a 10X objective (Fig. S5). The average values for height (H) and width (W) of the solid block, and height (H_w) and width (W_w) at the weld are similar within error (Fig. S5E). There is minimal variation in the dimensions at the weld versus that of the solid block. The optical images and profiles (Fig. S5B-D) show a small gap at both the edges of the weld, however the height profile (Fig. S5F) shows that the gap is on the surface and does not extend to the bottom. The surface roughness (root mean squared roughness, R_{RMS}) of the masters was measured at the weld site and to the right and left (Fig. S5G-H). The average roughness of the weld region was ±3.6 µm. The roughness of the regions to the left and right were also ±3.6 µm. The range measured was ±9.7 µm to ±0.3 µm. We also measured the average width fluctuations for three 3.5 mm segments that each contained one head to head weld. The average fluctuation was ±20 µm.

B5. UV-Visible Spectroscopy

UV-Visible spectroscopy was used to measure the absorbance of dye solutions inside PDMS microchannel networks. An Ocean Optics DH-mini UV-VIS-NIR source with a tungsten halogen light source and fiber optic cables was used to shine light through the channels, and an Ocean Optics USB2000+XR1-ES detector with a fiber optic cable was used to detect the light transmitted through the sample. Probes with convex lenses that have focal lengths of 1 cm were attached to the end of each fiber optic cable. The detector and source probe were positioned 2 cm apart and the device was positioned in between the probes (1 cm from each probe). A device with a standard channel height (path length of 200 ± 10 μm) that feeds into a taller channel (path length of 420 ± 10 μm) created by stacking blocks was used. Solutions of Indigo Carmine in nanopure water (18.2 MΩ) were prepared by serially diluting a stock, and these solutions were flowed through the device and absorbance was measured through standard height and taller height channels. The absorbance was measured seven times for each sample. An integration time of 8 ms, and boxcar width of 5 was used. Each measurement was an average of 4 scans. All measurements were corrected by using nanopure water as a blank solution.

B6. Complexometric iron quantification

On-chip detection of iron was done using the spectrometer with the same setup, as described in section B5. An integration time of 12 ms, and boxcar width of 3 were used. Each measurement was an average of 4 scans. Absorbance through a taller channel created by stacking blocks was measured and compared to absorbance in a cuvette. For on-device measurement, an aqueous iron solution was introduced through one inlet of a "Y" junction and a complexing agent through the second inlet. The standard solutions used were prepared from 250 mL of 0.00226 M ferrous ammonium sulfate, and the complexing reagent contained 100 mL of 10% 1,10-phenanthroline, 10 mL of hydroxylamine hydrochloride, and 40 mL of sodium acetate (calibration curves, Fig. S6). Unknown iron solutions were prepared by dissolving 50 mg of unknown sample from Thorn Smith Labs in 50 mL nanopure water (18.2 MΩ); three unknowns were quantified (2.14 %, 3.53 %, and 3.88 % verified independently by the vendor). Two peristaltic pumps were used to introduce the solutions into the device, each pump moved fluid into the device at a rate of 1.5 mL/min. The iron solution and complexing agent were mixed and the absorbance of the resulting rose colored solution was measured, and in between each measurement the device was flushed with a blank solution which contained hydroxylamine hydrochloride and sodium acetate dissolved in water. Each iron sample was measured for 1 minute and the device was then flushed with blank solution for 1 minute before switching to the next sample. For traditional in-cuvette measurements, the same solutions were mixed in flasks and used to obtain calibration/sample measurements using a bench-top spectrometer (Shimadzu UV-2501PC).

B7. High speed photography

High speed videos were captured using a Phantom Miro M310 high speed camera which was mounted on an Olympus IX81 microscope with an Olympus UPLFLN 4x objective (except for Video S9, which was mounted on Meiji Techno EMZ-13TR microscope, 4x objective). All videos were captured at 300 frames per second and a resolution of 1280×800 in raw Cine format.

B8. Droplet formation/analysis

The channels of the devices used as droplet generators/splitters were treated by flushing them with Aquapel and baking at 60° C for 20 minutes. Aqueous droplets contain 2% v/v Tween 20®. Droplet monodispersity was measured using ImageJ. Individual frames were captured from Videos S1, and S3 and then thresholded/converted to binary images. The binary images were analyzed using ImageJ's particle analysis function to automatically determine droplet areas, and major and minor axes of each droplet were measured. We assumed that droplets were ellipsoidal and that the minor axis of each droplet was equal to its out of plane diameter. Applying the formula for the volume of an ellipse we calculated the volumes for 50 droplets in fixed positions in the channels (marked on Fig. S5A, D).

Supporting Videos:

Video S1. **“**T” junction droplet generator in operation (real-time playback).

Video S2. A flow-focusing droplet generator in operation (real-time playback).

Video S3. Droplet splitting device in operation (real-time playback).

Video S4. Droplets flowing through defects in a channel, collected using a high-speed camera (0.1X playback).

Video S5. Droplets being split, collected using a high-speed camera (0.1X playback).

Video S6. Droplets generated by a flow-focusing device, collected using a high-speed camera (0.1X playback).

Video S7. Satellite droplet formation in a droplet splitter, collected using a high-speed camera (0.1X playback).

Video S8. Droplets flowing through a variable height channel (real-time playback).

Video S9. Droplet mixing in a multi-component device (real-time playback).

Video S10. Two-level channel network fabricated with bridge blocks (0.5X playback).

Video S11. A three-level fluidic device (0.5X playback).

Figure S1. Change in aspect ratio of the building blocks with thermal pressing. Topographic images of: (A) A standard building block after thermal pressing at 190° C for 12 minutes, (B) and a building block after thermal pressing for 25 minutes at 190° C (a 12 minute step to smooth the surface followed by a second 13 minute pressing step to mimic the welding step). (C) The change in dimensions of as-printed building blocks and for those following different amounts of thermal processing (sample 1 - untreated building block, sample 2 - pressed for 12 minutes, sample 3 – pressed for 25 minutes in a 12 minute step followed by a 13 minute step, sample 4 - pressed for 30 minutes in a 12 minute step followed by an 18 minute step, and sample 5 - pressed for 35 minutes in a 12 minute step followed by a 23 minute step). Sample 3 represents the standard experimental conditions—pressing and welding of blocks.

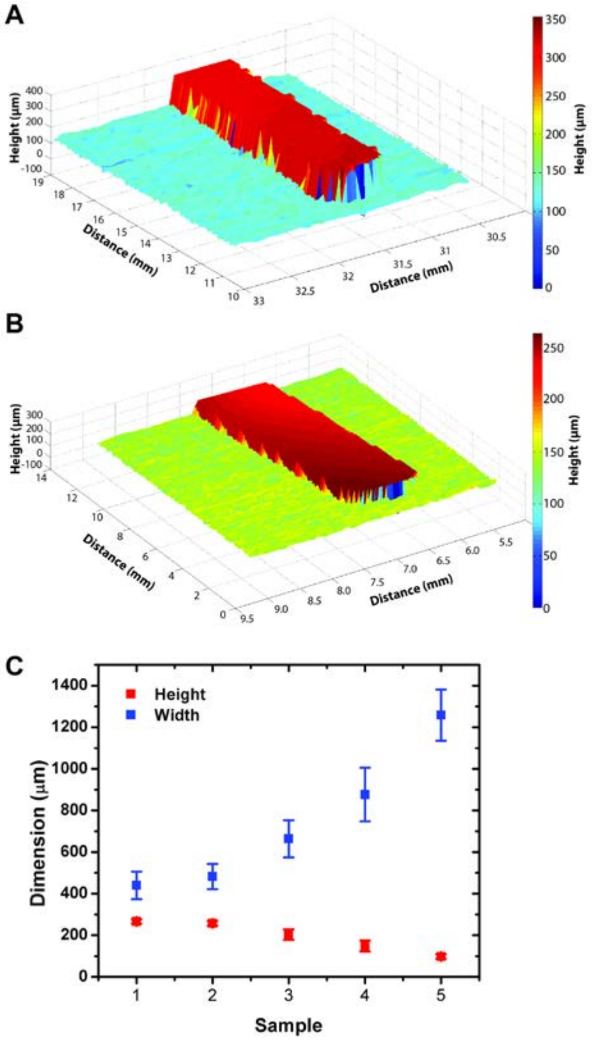

Figure S2. Analysis of masters produced using Teflon stencils as templates during welding. (A) A 45° template with unfused building blocks arranged inside. (B) Representative micrograph of a master that was thermally welded using the 45° template. (C) A 90° template with unfused building blocks arranged inside. (D) Representative micrograph of a master that was thermally welded using the 90° template. (E) Tabulated data for the angles achieved when welding blocks with stencil templates.

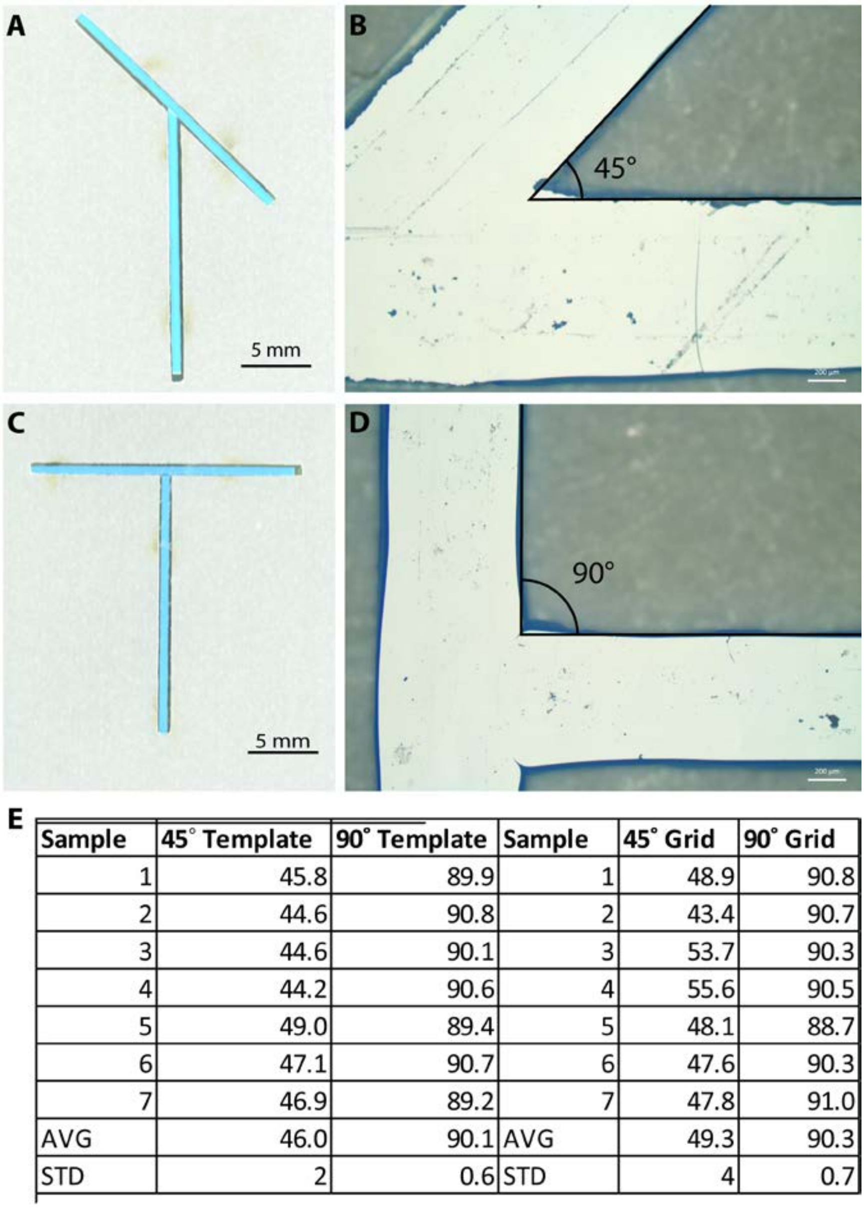

Sample	45° Template	90° Template	Sample	45° Grid	90° Grid
1	45.8	89.9	1	48.9	90.8
2	44.6	90.8	2	43.4	90.7
3	44.6	90.1	3	53.7	90.3
4	44.2	90.6	4	55.6	90.5
5	49.0	89.4	5	48.1	88.7
6	47.1	90.7	6	47.6	90.3
7	46.9	89.2	7	47.8	91.0
AVG	46.0	90.1	AVG	49.3	90.3
STD	2	0.6	STD	4	0.7

Figure S3. Analysis of the accuracy in block alignment in a manually assembled, rectilinear two-level device. Segments of the blue channel were analysed as follows: (i) each segment was annotated with a tangent line, (ii) a normal line was drawn for each tangent, and (iii) finally the angle between this normal line and the other tangents was measured. Δ_n is the difference between the measured angle θ_n and the ideal case, which would be 90°. Measurements for channels oriented along *x* are shown in black and those along *y* in red. The average difference in measured angles from the ideal case was $0.5_2 \pm 0.4°$.

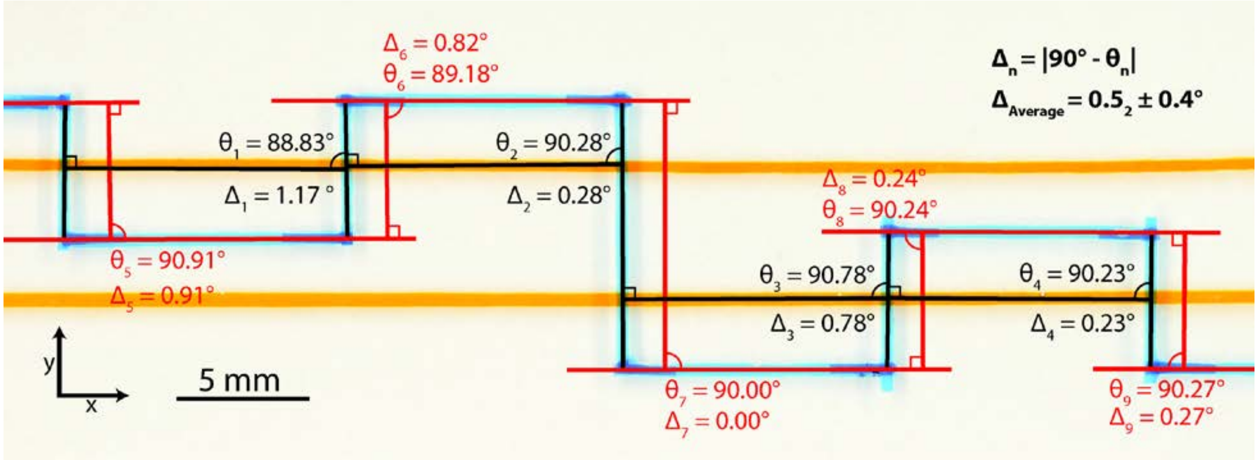

Figure S4. Load at breakage for welded building blocks. (A) Schematic showing the method of thermal pressing for the building blocks tested: 1) as-printed ABS block pressed at 190° C for 25 minutes, and 2) blocks pressed at 190° C for 12 minutes and then welded at 190° C for 13 minutes (weld site indicated by a dotted line). The right panels show a schematic for the measurement of load at breakage using a materials testing system. (B) Tabulated data for load at breakage for methods 1 and 2. (C) Plot showing the average load at breakage (n=7).

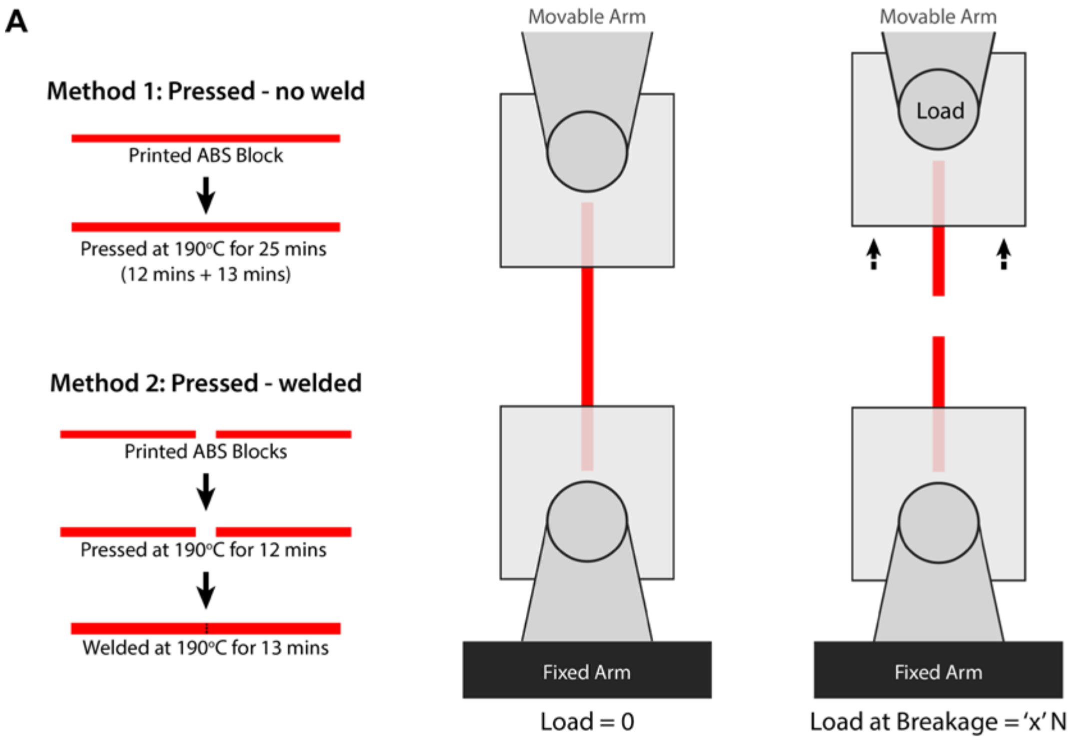

B

Pressed - no weld		Pressed - welded	
Sample #	**Load (N)**	**Sample #**	**Load (N)**
1	4.7	1	0.11
2	4.8	2	0.12
3	4.3	3	0.10
4	4.7	4	0.09
5	4.4	5	0.10
6	4.8	6	0.12
7	4.6	7	0.10
Avg.	4.6	**Avg.**	0.10
STD	0.2	**STD**	0.01

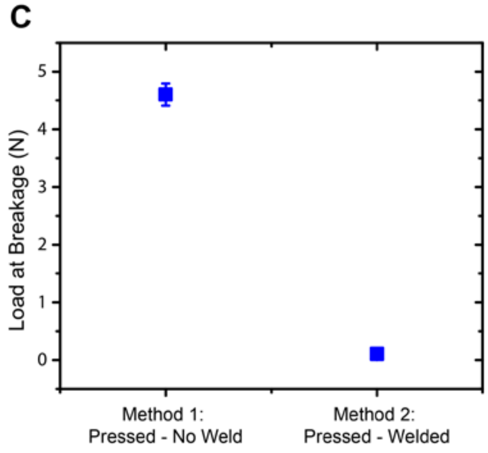

Figure S5. Dimension and cross-section analysis at welds. (A) Schematic illustration showing the different welds analyzed: (B, B’) Head-to-head weld, (C, C’) “T” configuration with straight-curved junction, and (D, D’) “T” configuration with straight-straight junction. (B-D) Optical micrographs and profiles generated using confocal microscopy for three different welds. (E) Dimensions at the weld and rest of the master (average of seven replicates). (F) Height profile at the head-to-head weld, scan indicated by the dotted line. (G) Representative optical micrograph showing three regions (at the weld and to the right and left) analyzed for root mean squared roughness (R_{RMS}). (H) Root mean squared roughness data for seven replicates of head-to-head welds (B, B’). (I-J) Width fluctuation analysis for three channel segments of 3.5 mm in length that each contain one to head-to-head weld; average values (N=3, 64 profiles each) are tabulated in J.

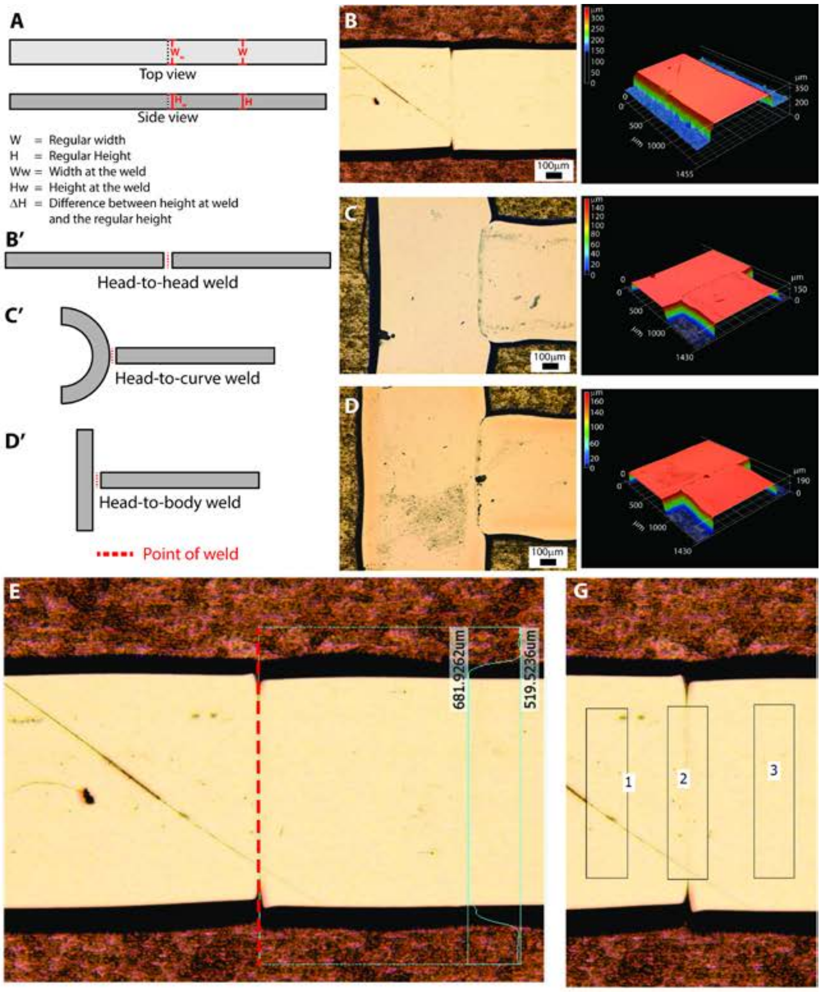

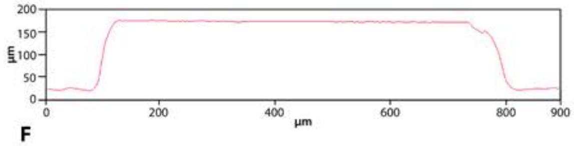

F

Sample Weld	W (µm)	H (µm)	W_w (µm)	H_w (µm)
Head-to-head weld	670 ± 20	180 ± 10	650 ± 20	180 ± 10
"T" Straight-curved weld	780 ± 50	150 ± 10	770 ± 80	150 ± 10
"T" Straight-straight weld	750 ± 60	170 ± 20	760 ± 90	160 ± 20

H

Sample #	R_{RMS} (µm)		
	#1	#2	#3
1	3.3	2.2	0.9
2	9.7	5.1	7.8
3	2.8	3.0	3.5
4	2.1	4.1	1.8
5	0.3	0.4	0.8
6	3.4	8.4	9.5
7	1.2	1.7	2.1
Avg.	3.3	3.6	3.8

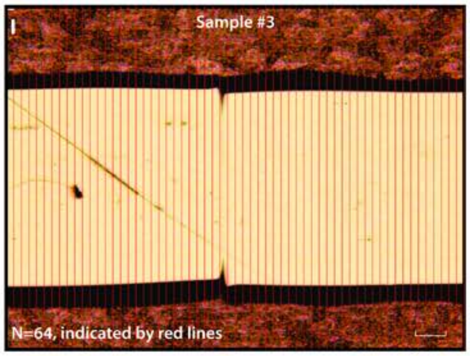

J

Sample	Average Width (µm, N=64)	STD
#1	64_1	2_3
#2	66_4	1_4
#3	677	8
Average	660	20

Figure S6. Typical defects in microchannels fabricated with building-block-based masters. (A-D) Micrographs of the segment of each microfluidic device where representative defects were observed. Inset are schematic illustrations of the area in the master assembly where the defect occurred. (A) A defect between two welded blocks squeezes a droplet, which continues past. (B) Defects along the walls of the channels at the point where droplets are divided. (C) Defects along the channel walls of a flow focusing droplet generator where droplets are formed. (D) Defects along the channel walls causing the formation of satellite droplets (annotated in red).

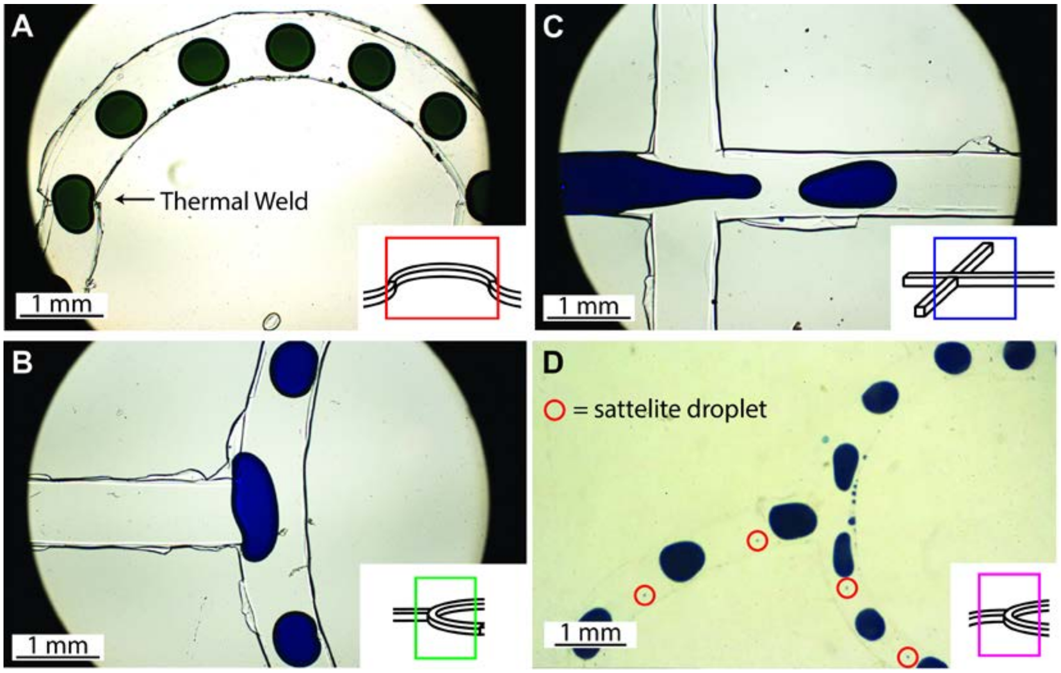

Figure S7. Micro-droplet analysis for monodispersity. (A) Top-down photograph of a droplet splitter, (B) a representative thresholded image, and (C) outlines of droplets. (D) Top-down photograph of a "T" junction droplet generator, (E) a representative thresholded image, and (F) outlines of droplets. The arrows indicate the position at which the individual droplets were analyzed during flow. 50 different droplets were analyzed at the position of each arrow and the average volumes were estimated to be 140 ± 7 nL, 64 ± 3 nL, 78 ± 3 nL, and 114 ± 9 nL for droplet positions 1-4 respectively. All scale bars are 5 mm.

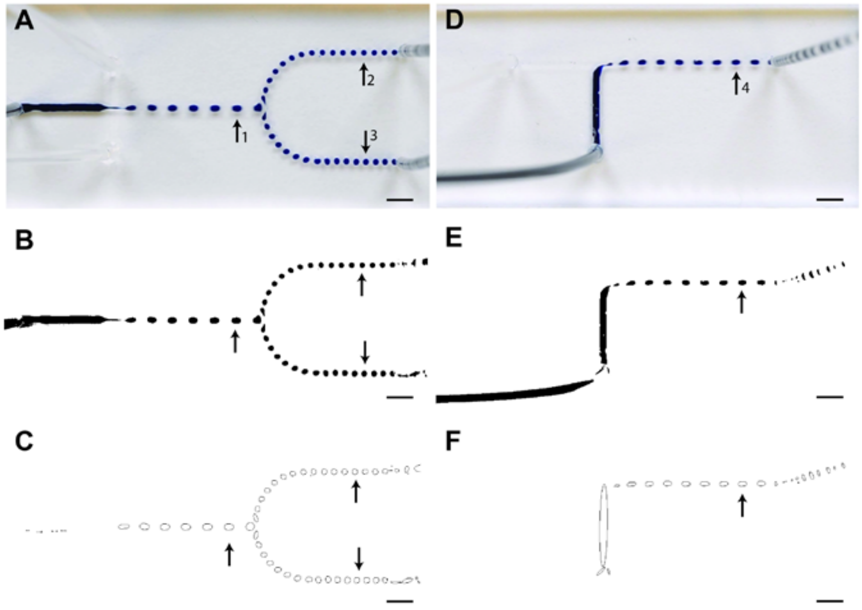

Position 1	Position 2	Position 3
Average Volume nL (n=50)		
140	64	48
Standard Deviation		
7	3	3
Coefficient of Variation %		
4.7	4.7	4.2

Position 4
Average Volume nL (n=50)
114
Standard Deviation
9
Coefficient of Variation %
7.7

Figure S8. Calibration Curves for ferroin. (A) Generated from measurements on-device in flow, and (B) generated in a cuvette using a bench-top spectrometer.

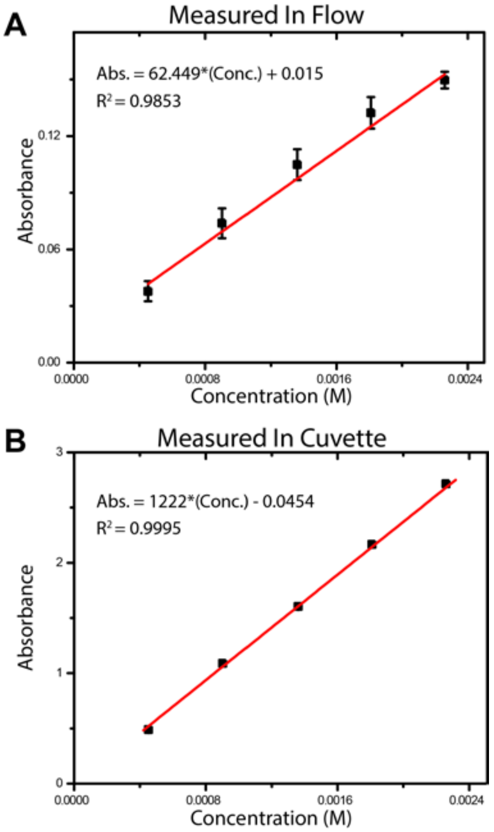

References

1 J. C. McDonald, M. L. Chabinyc, S. J. Metallo, J. R. Anderson, A. D. Stroock and G. M. Whitesides, *Anal. Chem.*, 2002, **74**, 1537-1545.

2 H. Makamba, J. H. Kim, K. Lim, N. Park and J. H. Hahn, *Electrophoresis*, 2003, **24**, 3607-3619.